Thermal conductivity/structure correlations in thermal super-insulating pectin aerogels

Sophie Groult, Tatiana Budtova

Carbohydrate Polymers, **196**, 73–81 (2018) DOI: 10.1016/j.carbpol.2018.05.026

Thermal conductivity/structure correlations in thermal super-insulating pectin aerogels

Sophie Groult, Tatiana Budtova*

MINES ParisTech, PSL Research University, Center for Materials Forming (CEMEF),

UMR CNRS 7635, CS 10207, 06904 Sophia Antipolis, France

Corresponding author: Tatiana Budtova

email: Tatiana.budtova@mines-paristech.fr

tel : +33 4 93 95 74 70

Sophie Groult: Sophie.Groult@mines-paristech.fr

Highlights

- Pectin aerogels with thermal conductivity below air were prepared and characterized
- The influence of pectin concentration, pH and presence of calcium was studied
- Calcium cross-linked pectins formed gels, shrank less and showed the lowest density
- Pectin aerogels from solutions were mesoporous and with lowest conductivity

Abstract

Pectin aerogels were synthesized via dissolution-solvent exchange-drying with supercritical CO_2. The goal was to correlate thermal conductivity with aerogel morphology and properties in order to understand how to obtain a thermal super-insulating material with the lowest possible conductivity. Polymer concentration, solution pH and presence of bivalent ions were varied to tune pectin gelation mechanism and the state of matter, solution or gel. For the first time for bio-aerogels, a U-shape curve of thermal conductivity as a function of aerogel density was obtained. It shows that to reach the lowest conductivity values, a compromise between density and pore sizes is needed to optimize the inputs from the conduction of solid and gaseous phases. The lowest value of conductivity, 0.015 W/m.K, was for aerogels from non-gelled pectin solutions. Calcium-induced gelation leads to pectin aerogels with very low density, around 0.05 g/cm^3, but with many macropores, thus reducing the contribution of Knudsen effect.

Key words: pectin; aerogel; thermal conductivity; density; specific surface area

1. Introduction

Aerogels are lightweight nanostructured materials composed of a solid network with open porosity. Classical aerogels, known since the pioneering work of Kistler, are based on silica (Kistler, 1931). They have outstanding properties such low density (0.05 - 0.1 g/cm^3) and very high specific surface area (800 - 1000 m²/g and higher). Thanks to these properties, silica aerogels are thermal super-insulating materials, *i.e.* with thermal conductivity below that of air in ambient conditions, 0.013 – 0.014 vs 0.025 W/m.K. Till now, silica aerogels are known to be materials with the lowest thermal conductivity. Some synthetic polymer aerogels, for example, based on polyurethanes, are also super-insulating materials but with slightly higher conductivity, around 0.017 W/m.K (Diascorn, Calas, Sallee, Achard, & Rigacci, 2015).

Bio-aerogels are the third generation of aerogels: they are made of natural polymers such as polysaccharides and proteins (Chtchigrovsky et al., 2009; Druel, Bardl, Vorwerg, & Budtova, 2017; Gurikov, Raman, Weinrich, Fricke, & Smirnova, 2015; Horvat, Fajfar, Uzunalić, Knez, & Novak, 2017; Jiménez-Saelices, Seantier, Cathala, & Grohens, 2017; Kobayashi, Saito, & Isogai, 2014; Quignard, Valentin, & Di Renzo, 2008; Rudaz et al., 2014; Seantier, Bendahou, Bendahou, Grohens, & Kaddami, 2016; Selmer, Kleemann, Kulozik, Heinrich, & Smirnova, 2015; Sescousse, Gavillon, & Budtova, 2011). Kistler reported the possibility of making aerogels from gelatin, cellulose, nitrocellulose, agar and egg albumin (Kistler, 1931), but their properties were not reported. The synthesis of bio-aerogels is inspired by that of classical aerogels: from polymer dissolution to solution gelation (in some cases this step can be omitted (Buchtová & Budtova, 2016; Gurikov & Smirnova, 2018; Horvat et al., 2017; Innerlohinger, Weber, & Kraft, 2006; Pircher et al., 2016; Sescousse et al., 2011; Tkalec, Knez, & Novak, 2015)) followed by solvent exchange and drying with super-critical (sc) carbon dioxide. Compared to silica aerogels which are extremely fragile, bio-aerogels do not break under compression (Rudaz et al., 2014). Moreover, the synthesis of

bio-aerogels does not involve any toxic compounds which is the case of many synthetic polymer aerogels (for example, based on resorcinol formaldehyde or polyurethanes cross-linked with isocyanate). These properties make bio-aerogels "human-friendly" and thus very attractive in life-science applications (García-González, Alnaief, & Smirnova, 2011; Veronovski, Tkalec, Knez, & Novak, 2014).

Very few is known about the thermal conductivity of bio-aerogels, and practically nothing on conductivity-structure correlations. Thermal super-insulating bio-aerogels with the conductivity around 0.016−0.020 W/m.K were reported for aerogels based on pectin (Rudaz et al., 2014), nanofibrillated cellulose (Jiménez-Saelices et al., 2017; Kobayashi et al., 2014; Seantier et al., 2016), alginate (Gurikov et al., 2015) and starch (Druel et al., 2017). In the first approximation, thermal conductivity λ of porous materials is an additive sum of solid λ_{solid} and gaseous λ_{gas} phases' conduction and of the radiative heat transfer λ_{rad}:

$$\lambda = \lambda_{solid} + \lambda_{gas} + \lambda_{rad} \quad (1)$$

Solid phase conduction logically increases with density increase. To minimize the conduction of the gaseous phase two options are possible: either evacuation the gas (air), or decrease of pores' sizes down to mesoporous region. In the latter case pore size is below the mean free path of air molecules, which is around 70 nm at 25 °C and 1 atm, leading to λ_{gas} lower than that of ambient air according to Knudsen effect. λ_{rad} is not significant at room temperatures and optically thick materials. Intuitively it is thus clear that the lowest thermal conductivity can be reached for low-density mesoporous materials. For silica aerogels it was demonstrated that the dependence of thermal conductivity on density has a U-shape (Hüsing & Schubert, 1998): higher density leads to conductivity increase because of λ_{solid} input, and lower density leads to λ_{gas} increase because of the presence of large pores which do not contribute to Knudsen effect.

Bio-aerogels from medium and high methylated pectins were shown to be thermal super-insulating materials with conductivity increasing from 0.018 W/m.K to 0.03 W/m.K for densities from 0.05 to 0.15 g/cm^3 (Rudaz et al., 2014). Polymer concentration was varied to modify aerogel density but no U-shape curve was obtained. Similar results but with slightly higher conductivity values were recorded for starch aerogels (Druel et al., 2017). Only one publication reports a U-curve of conductivity vs density for freeze-dried bleached cellulose fibers "filled" with nanofibrillated cellulose (Seantier et al., 2016): density was varied by sample compression and the lowest thermal conductivity was 0.023 W/m.K. The correlations between the conductivity and structure and properties of bio-aerogels made via dissolution-solvent exchange route remain open.

Pectin is mainly polygalacturonic acid esterified (methylated, acetylated or amidated) to different degrees, usually extracted from citrus peel or apple pomace. Depending on the intrinsic properties of the polymer and external conditions (pH, temperature, ionic strength, presence of multivalent metal ions, sugars, etc) pectin chains in aqueous solutions may associate in different ways leading to the formation of various types of gels. The goal of this work was to tune pectin aerogels properties and morphology and correlate them with thermal conductivity. We shall demonstrate that by adjusting polymer concentration, pH and presence of calcium it is possible to counter balance the thermal contributions of solid and gaseous phases and obtain the optimal (minimum) value of thermal conductivity.

2. Experimental

2.1. Materials

Pectins used in the work were all from citrus, with different degrees of esterification DE (as given by providers): with DE 35% (named as P35), 56 % (P56), 59 % (P59) and 70 % (P70). P35, P59 and P70 were kindly provided by Cargill, and P56 was purchased from Sigma

Aldrich. Most of the work was performed on P35 in what concerns the influence of pectin concentration, pH and concentration of calcium. The other pectins, P56, P59 and P70, were dissolved only at pH 1 and 3 wt% for comparison with P35. Ethanol (purity > 99%, Laboratory Reagent Grade) and hydrochloric acid (32%, Analysis Grade, Certified Analytical Reagent) were from Fisher Scientific and used as received. Calcium chloride anhydrous powder (96% extra pure) from Acros Organics was used to make $CaCl_2$ solutions. Water was distillated.

2.2. Methods

2.2.1. Preparation of pectin aerogels

Pectin aerogels, also called "aeropectins", were synthesized via dissolution, gelation (in some cases non-gelled solutions were used), solvent exchange and drying with sc CO_2. Pectin aqueous solutions were prepared by mixing pectin powder and water at 65 °C under stirring at around 400 rpm during 4 to 5 hours. Pectin concentrations are given in wt%. After complete dissolution, solution pH, initially around 3, was adjusted by addition of HCl. pH was varied from 1 to 3 because at pH ≥ 4 solutions were of so low viscosity that solvent exchange was not possible. More details will be given in Results section. Solutions were then poured into a mold (dimensions of dry samples depend on characterization method and will be given later), in some cases $CaCl_2$ solution was added to induce ionic gelation. The molar ratio R of calcium to pectin carboxyl groups was calculated as follows:

$$R = \frac{[Ca^{2+}]}{[RCOO^{-}]} \qquad (2)$$

where concentrations are expressed in $mol.L^{-1}$. In this study, R was varied from 0.05 to 0.2. It was not possible to prepare homogeneous gels at pH > 3 cross-linked by calcium because of the instantaneous gelation leading to highly heterogeneous samples.

Pectin solutions were kept for 48 h at room temperature. Depending on the conditions (pH, presence of $CaCl_2$) solutions were gelling or not as determined by a simple "tilting test"; the state of matter, solution (noted "S" for the matter flowing) or gel (noted "G" for the matter not flowing) will be given for each aerogel studied.

In order to perform drying with sc CO_2, water has to be replaced by a fluid which is miscible with CO_2. Ethanol was used for this purpose: solvent exchange was performed by progressively decreasing water/ethanol (v/v) ratio to 50/50, 25/75 and 0/100, followed by extensive washing with pure ethanol. For the case when the state of matter was "gel", the sample was placed in water-ethanol baths as described above. When the state of matter was "solution", a mixture of water-ethanol 50/50 (v/v) was gently put on the top of the solution (Figure S1a in Supplementary Material). This led to a non-solvent induced phase separation (Figure S1b) also known as "immersion precipitation" process in membranes' preparation (Wijmans, Altena, & Smolders, 1984; Wijmans, Baaij, & Smolders, 1983): the solubility of the polymer decreases as non-solvent proportion increases. This process had already been reported for making bio-aerogels from cellulose-ionic liquid (1-ethyl-3-methylimidazolium acetate (EmimAc): (Buchtová & Budtova, 2016; Pircher et al., 2016; Sescousse et al., 2011), hot cellulose-N-methyl morpholine-N-oxide monohydrate (NMMO) (Innerlohinger et al., 2006), alginate (Gurikov & Smirnova, 2018; Horvat et al., 2017; Tkalec et al., 2015) and pectin solutions (Horvat et al., 2017; Tkalec et al., 2015). In both cases, solution or gel, pectin coagulated during solvent exchange step resulting in 3D pectin "alcogel". The latter were then dried with sc CO_2 (see details on drying parameters in (Druel et al., 2017)).

In most of the cases dried samples were disks with diameter around 18-25 mm and thickness around 7-10 mm. For the measurements of thermal conductivity the samples were disks of diameter around 40 - 60 mm and thickness around 5 - 10 mm. Exact final dimensions

depended on sample shrinkage (see photos of pectin aerogels in Figure S2 of the Supplementary Material). All aerogels were produced at least in triplicate.

2.2.2. Characterisation

Molecular weight of pectins. Pectins' intrinsic viscosities were determined using Huggins approach by measuring kinematic viscosity of diluted pectin solutions (dilutions in series from 0.15 wt% to 0.05 wt%) in saline conditions (0.01 mol/ L of NaCl) at 26.6°C, with capillary viscometer iVisc from LAUDA, Ubbelhode Dilution Viscometer Type I with capillary diameter 0.63 mm. These conditions allowed calculation of pectin molecular weight accoding to (Masuelli, 2014).

Volume shrinkage and density. Volume shrinkage was determined after solvent exchange and after sc drying (V_f) according to the following equation:

$$\text{Volume shrinkage, \%} = \frac{V_i - V_f}{V_i} \times 100\ \% \qquad (3)$$

where V_i is the volume of the gel before solvent exchange.

The skeletal density (ρ_{sk}) of aerogels was measured using AccuPyc 1330 Pycnometer from Micromeritics, ρ_{sk} = 1.5 g/cm^3. Bulk density (ρ_{bulk}) was determined as the ratio of sample mass to volume. The mass of the aerogel was measured with digital analytical balance with a precision of 0.01 mg. The volume was measured with digital caliper.

Porosity P and pore volume V_p were determined as follows:

$$P\ \% = 1 - \frac{\rho_{bulk}}{\rho_{sk}} \times 100\% \qquad (4)$$

$$V_p\ (\text{cm}^3/\text{g}) = \frac{1}{\rho_{bulk}} - \frac{1}{\rho_{sk}} \qquad (5)$$

Specific surface area (S_{BET}) was determined by nitrogen adsorption and BET method using Micromeritics ASAP 2020. Prior to analysis, samples were degassed in a high vacuum at 70 °C for 10 h.

It should be noted that standard methods for measuring pore size distribution and pore volume such as BJH approach (nitrogen adsorption) or mercury porosimetry cannot be applied to bio-aerogels. BJH method considers pores sizes below 200 nm, which takes in account around 10-20% of the total pore volume (Rudaz et al., 2014). The classical formula for calculating average pore size D within the approximation of cylindrical pores, $D = 4V_{p,BJH}/S_{BET}$, where $V_{p,BJH}$ is pore volume measured by nitrogen adsorption/desorption method, thus gives strongly underestimated values of D. If replacing $V_{p,BJH}$ by V_p calculated from skeletal and bulk densities, D is strongly overestimated as far as S_{BET} considers only mesopores and small macropores. When mercury porosimetry is used, bio-aerogels are compressed without mercury penetration in the pores, and thus the "value" given by the machine is an artefact (Rudaz, 2013; Rudaz et al., 2014). It may also be possible that bio-aerogel is compressed at higher nitrogen pressure. An example of BHJ analysis of one of aeropectins obtained in this work is shown in Figure S3 of the Supplementary Material. It shows that $V_{p,BJH}$ is around 8 % of V_p. Thus we prefer not to speculate on the pore sizes, and we illustrate aerogels' morphology with scanning electron microscopy.

Thermal conductivity (λ) of pectin aerogels was measured at ambient pressure using heat flow meter Fox 150 equipped with a custom "micro flow meter cell" developed for small samples (see details in (Rudaz et al., 2014)) at 20°C. Spaceloft® aerogel from Aspen (thickness of 3.70 mm) with thermal conductivity of 0.0133 W/(m.K) at 20°C according to the European Norm EN 12667 was used as a standard for calibration.

The morphology of aerogels was examined using Supra40 Zeiss SEM FEG. A layer of 7 nm of platinum was sputtered using a Q150T Quarum metallizer.

3. RESULTS

3.1. Molecular weight of pectins

The intrinsic viscosities of P35, P59 and P70 were 340 cm^3/g, 502 cm^3/g and 566 cm^3/g, respectively. Molecular weights of pectins were calculated using Mark-Houwink-Sakurada equation:

$$[\eta] = K M^a \quad (7)$$

where K = 0.0234 and a = 0.8221 according to (Masuelli, 2014). The molecular weights were 1.15 10^5 g/mol for P35, 1.86 10^5 g/mol for P59 and 2.15 10^5 g/mol for P70.

3.2. Thermal conductivity as a function of pectin aerogel density: summary of all results

As mentioned in the Introduction, thermal conductivity of aerogels is strongly impacted by network morphology and density. We modified aeropectins' structural properties by varying key synthesis parameters: solution pH, pectin concentration and presence of calcium ions. All results on thermal conductivity obtained in this work are summarized in Figure 1 as a function of aeropectin bulk density and all characteristics of aerogels are in Table S1 of the Supplementary Material. Figure 1 shows, for the first time, a U-shape curve obtained for this type of bio-aerogels. The general trends known for thermal conductivity of classical aerogels are thus applicable to bio-aerogels. The minimal thermal conductivity is very low, 0.015 W/m.K, and comparable with that of silica aerogels; it corresponds to pectin aerogel density of 0.1 g/cm^3 (Figure 1).

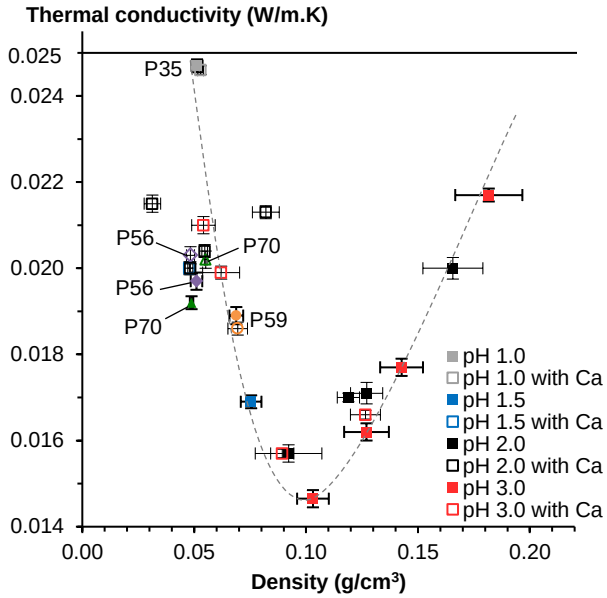

Figure 1

Aeropectin thermal conductivity as a function of density. Open points correspond to samples cross-linked with calcium. Not-marked samples are from P35 (squares). P56 (diamonds), P59 (circles) and P70 (triangles) were made from 3 wt% pectin solutions at pH 1. Solid line is conductivity of air in ambient conditions; dashed line is given to guide the eye.

Figure 1 shows that density is one of the key parameters controlling thermal conductivity, as expected. Thus the first question to answer is what are the experimental conditions which control the density of aeropectin? For example, when density varies from 0.05 to 0.10 g/cm^3, thermal conductivity decreases from 0.024 to 0.015 W/m.K. Obviously, the morphology of aerogels also plays a very important role. Thus the second question to answer is how to control the morphology of aeropectins to obtain the lowest thermal conductivity? To answer these questions we studied the influence of P35 concentration, pH, concentration of Ca^{2+} ions and state of matter (gel or solution) before solvent exchange on aeropectin density and specific surface area to finally correlate with thermal conductivity.

3.2. Influence of pectin concentration on aerogel density and morphology

An example of the influence of pectin concentration on aerogel density and specific surface area is illustrated in Figure 2. All solutions were made at pH 2. Samples' shrinkage after solvent exchange and after drying is shown in Figure S4 of the Supplementary Material. Increasing pectin concentration decreased shrinkage, as already reported for other bio-aerogels (Buchtová & Budtova, 2016; Hoepfner, Ratke, & Milow, 2008). The values obtained in this work are from 65 % to 80 % for non-cross-linked samples, and from 30 % to 50 % for cross-linked with calcium. Despite lower shrinkage at higher polymer concentration, aeropectin density increased with the increase of pectin concentration in both cases, when pectin was cross-linked with calcium and not. Similar results were obtained at pH 3 (Figure S5 of the Supplementary Material). It should be noted that the density of cross-linked aeropectins was twice lower than that of the corresponding non-cross-linked ones, and it was very close to the theoretical density calculated for the case of zero volume shrinkage (solid line in Figure 2).

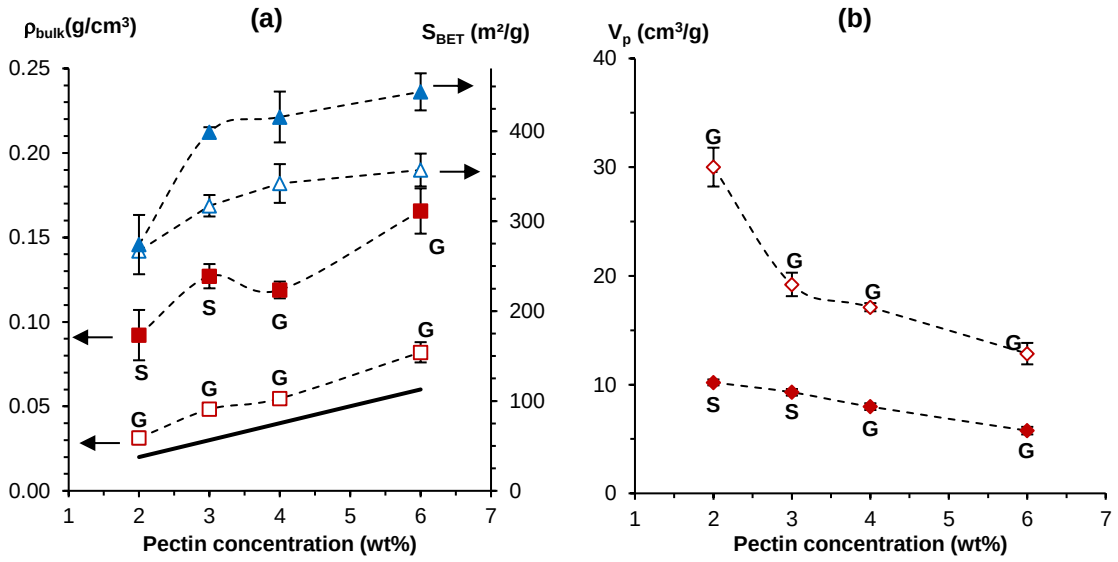

Figure 2

(a) Density (squares) and specific surface area (triangles) and (b) pore volume of aeropectins based on P35 dissolved at pH 2 as a function of polymer concentration in solution. Filled

points correspond to non-cross-linked samples, open points – when calcium was added (R = 0.2). Solid line is theoretical density corresponding to zero volume shrinkage. The state of matter before solvent exchange is indicated for each case (solution "S" or gel "G"). Dashed lines are given to guide the eye.

Specific surface area also increased with pectin concentration (Figure 2, triangles) with highest values being around 360 and 440 m^2/g for cross-linked and non-cross-linked pectins, respectively. Much higher S_{BET} were obtained at pH 3 (Figure S5 of the Supplementary Material), up to 600 ± 15 m^2/g. To the best of our knowledge, this is the highest value ever obtained for pectin aerogels (García-González et al., 2011; García-González, Jin, Gerth, Alvarez-Lorenzo, & Smirnova, 2015; Rudaz et al., 2014; Veronovski et al., 2014; White, Budarin, & Clark, 2010). The increase of specific surface area with polysaccharide concentration had already been reported previously (Buchtová & Budtova, 2016; Jin, Nishiyama, Wada, & Kuga, 2004). As suggested in (Buchtová & Budtova, 2016), the increase of polymer concentration leads, in the first approximation, to the decrease of pore size without significant evolution of pore walls' thickness. In other words, the addition of matter leads to a division of pores into smaller ones.

An example of morphology of aeropectins made from solutions of various initial pectin concentrations and cross-linked with calcium (R = 0.2) is presented in Figure 3. With the increase pectin concentration the network becomes denser and pores smaller, confirming the trend obtained on specific surface area (Figure 2).

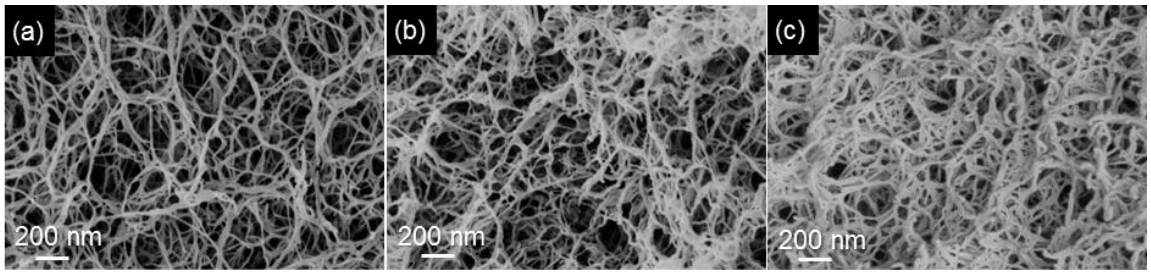

Figure 3

SEM images of P35 based aeropectins from 2 wt% (a), 4 wt% (b) and 6 wt% (c) solutions at pH 2 cross-linked with calcium (R = 0.2).

The results presented above show that the increase of pectin concentration leads to the increase in density and decrease of network pore size. The first trend should logically result in the enhancing of heat conduction via the solid backbone, and thus to the overall increase in thermal conductivity. The increase of thermal conductivity as a function of density is given as an example for pH 2 and 3 in Figure S6 of the Supplementary Material. The second trend leads to the increase of the amount of mesopores which contribute to Knudsen effect, and thus to the decrease of the conduction of gaseous phase. These two oppositely acting trends may result in different behaviour of thermal conductivity as a function of polymer concentration depending which input is dominating. Figure 4 shows that for aeropectins cross-linked with calcium thermal conductivity weakly depends on polymer concentration, with a small minimum at 3 wt%, indicating that density increase is counterbalanced by pore's size decrease in their inputs in the overall conductivity. On the contrary, for non-cross-linked samples the increase of polymer concentration leads to the increase of the conductivity. It is thus clear that in addition to polymer concentration, cross-linking strongly influences aeropectin morphology and thus thermal conductivity. The effect of pH and presence of calcium on aeropectin properties is presented and discussed below.

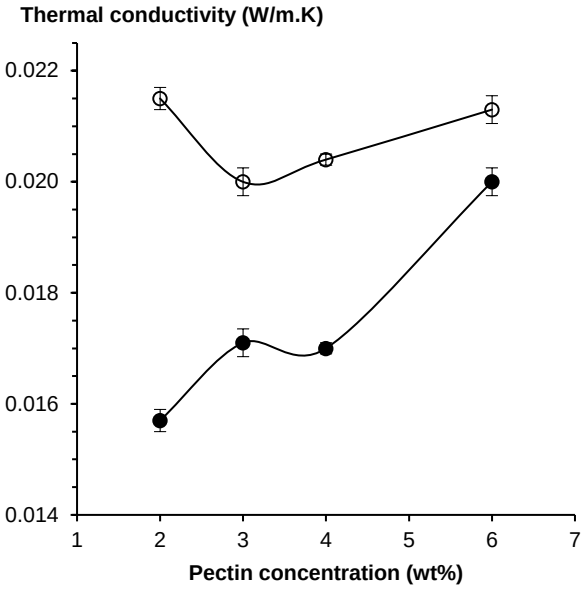

Figure 4

Thermal conductivity of P35 aeropectin as a function of polymer concentration, at pH 2, cross-linked with calcium (open points) and not (filled points). Lines are given to guide the eye.

3.3. Influence of Ca-induced cross-linking and pH on pectin aerogel properties

It is well known that pH and presence of metal ions, especially bivalent, influence pectin solution viscosity and gelation (Thakur, Singh, & Handa, 1997; Walkinshaw & Arnott, 1981). First, we will examine how aeropectin density, morphology and thermal conductivity change with solution pH keeping pectin and calcium concentration constant, and then calcium content will be varied at constant pectin concentration and pH.

3.3.1. Influence of pH at R = 0 and 0.2

At low pH gelation of pectin solution occurs due to intermolecular hydrogen bonding between protonated groups (carboxyl, hydroxyl), and stabilized by hydrophobic interactions of methylated groups (Oakenfull & Scott, 1984; Gilsenan, Richardson, & Morris, 2000;

Voragen, Schols, & Visser, 2003). The increase of pH leads to deprotonation of acid groups and thus prevents chains' aggregation and gelation. The addition of calcium is known to induce ionic gelation which is more pronounced when i) lowering pectin DE (Burchard & Ross-Murphy, 1990), ii) increasing calcium concentration (Fraeye et al., 2009; Löfgren, Walkenström, & Hermansson, 2002), and iii) when solution pH is close and higher than pKa (Gidley, Morris, Murray, Powell, & Rees, 1980), for pectins pK_a is around 3 - 3.5 depending on the degree of esterification (Ralet, Bonnin, & Thibault, 2002; Ralet, Dronnet, Buchholt, & Thibault, 2001). To understand the influence of pH, presence of calcium and state of matter (solution or gel) on aerogel morphology and thermal conductivity we varied pH, from 1 to 3, and for each pH two types of samples were prepared, without and with calcium (R = 0.2).

Pectin shrinkage after solvent exchange and after drying as a function of pH is presented in Figure S7 (Supplementary Material), and aeropectin density and specific surface area in Figure 5a and 5b, respectively. For the samples cross-linked with calcium no influence of pH on shrinkage was recorded (around 40 %), within the experimental errors. The total shrinkage of non-cross-linked samples shows a strong dependence on pH, from 50% to 80 % for pH from 1 to 3, respectively. This trend is reflected by density which does not vary with pH for cross-linked pectin aerogels and increases with pH in almost 3 times for non-crosslinked ones (Figure 5a). Due to the strength of the bonds, ionic gelation leads to more firm and brittle gels than their physical counterparts (Djabourov, Nishinari, & Ross-Murphy, 2013). In particular, it is well known that low methylated pectins undergo a strong ionic gelation in the presence of calcium due to their high sensitivity to Ca^{2+} ions; these pectins were also reported to to form weak acid gels in the absence of cations at pH values below pk_a (Morris, Gidley, Murray, Powell, & Rees, 1980; Gilsenan et al., 2000; Löfgren et al., 2002; Lootens et al., 2003; Capel, Nicolai, Durand, Boulenguer, & Langendorff, 2006; Ström, Schuster, & Goh, 2014). Moreover, the strength of pectin gel cross-linked with calcium increases with calcium

concentration up to a certain value, generating a denser pectin network (Fraeye et al., 2009; Fraeye, Duvetter, Doungla, Van Loey, & Hendrickx, 2010; Löfgren et al., 2002; Lootens et al., 2003). Our results confirm the trends reported for gels: cross-linked pectins (here, at R = 0.2) are the most "resistant" to solvent exchange and drying and thus show the lowest shrinkage and density. For P35 3 wt% solutions all cross-linked pectins were gels before solvent exchange while non-cross-linked pectins were gels only at low pH, 1 and 1.5, and solutions at pH 2 and 3 (Figure 5a). It should be noted that gelation of pectin solutions is concentration-dependent: low pH induces thermal gelation if the number of the effective interactions is sufficient. For example, for P35 at pH 2 gelation occurred for 6 wt% and 4 wt% solutions but not for 3 wt% or 2 wt% (Figure 2).

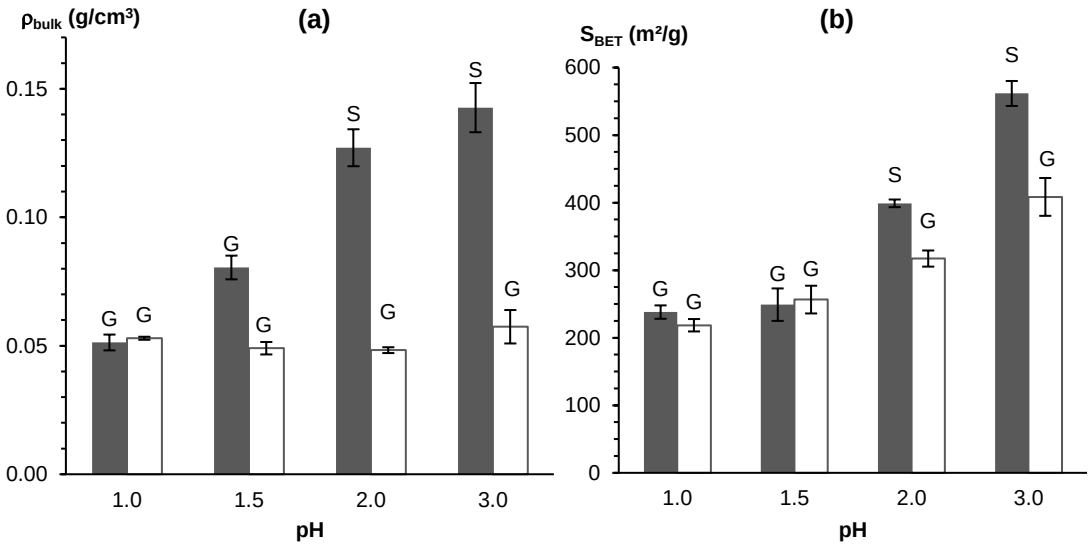

Figure 5

Aeropectin density (a) and specific surface area (b) as a function of pH, cross-linked with calcium (R = 0.2) (white bars) or not (black bars), from P35 dissolved at 3 wt%. The state of matter before solvent exchange is indicated for each case (solution "S" or gel "G").

One of the interesting features is that the addition of non-solvent to non-gelled pectin solutions does not lead to polymer total collapse, which is the case for many synthetic flexible polymers. Despite strong volume decrease, pectin results in 3D "wet" network after solvent exchange and in aerogels with rather low density, 0.10 – 0.15 g/cm^3 (Figure 2 and 5). This phenomenon had already been reported for several bio-aerogels synthesized from non-gelled polysaccharide solutions (Buchtová & Budtova, 2016; Gurikov & Smirnova, 2018; Horvat et al., 2017; Innerlohinger et al., 2006; Pircher et al., 2016; Sescousse et al., 2011; Tkalec et al., 2015). Overall, the process is similar to the formation of membranes via phase inversion, but drying with sc CO_2 results in highly porous open-pore network with thin pore walls.

The kinetics of polysaccharide coagulation from solution or gel when immersed in a non-solvent was studied in details for the case of cellulose when dissolved in NMMO (Biganska & Navard, 2005; Laity, Glover, & Hay, 2002) (here, solution is in solid state at room temperature), in ionic liquid EmimAc (Hedlund, Köhnke, & Theliander, 2017; Sescousse et al., 2011) (solution) and in 8%NaOH-water (gel) (Gavillon & Budtova, 2007). The process was shown to be described by Fickian diffusion with cellulose solvent molecules moving out of solution or gel and non-solvent (here, water) molecules diffusing in the sample. While the morphology of coagulated (or precipitated) cellulose with non-solvent in the pores differs for the cases when the state of matter is "liquid" or "solid" solution or gel, all studies agree that structure formation occurs via phase separation.

Polymer, and, in particular, pectin chains, are aggregating upon the addition of non-solvent forming a network of coagulated polymer with non-solvent in the pores. We hypothise that the reason of pectin's "resistance" to collapse in a non-solvent is chain semi-rigidity; and very slow kinetics of phase separation could also play a role in structure stabilisation. Most of bio-aerogels reported in literature are made either from gelled solutions (alginate, starch, carrageenan, chitosan, cellulose-NaOH) or solidified solutions (cellulose-NMMO

monohydrate, cellulose-1-butyl-3-methylimidazolium chloride), and thus the phenomenon of polysaccharide chains' aggregation from dissolved to coagulated state during solvent exchange is not discussed as far as network structure is already formed. Molecular modeling could be helpful to better understand and predict the morphology of bio-aerogels prepared via different synthesis routes.

Figure 5b represents specific surface area of pectin aerogels which density is shown in Figure 5a. S_{BET} significantly increases with pH for both cross-linked and non-cross-linked aeropectins. Aerogels made from cross-linked and physical gels at low pH, 1 and 1.5, show the same S_{BET}, while aerogels from solutions at pH 2 and 3 show S_{BET} much higher than that from cross-linked pectins. Several factors have to be taken into account to explain S_{BET} results:

- At very low pH all acidic groups of galacturonic acid are protonated. This results in only a very small number of groups that remain charged and thus able to interact with calcium ions; the influence of calcium is thus minor. The gel was formed due to the formation of junction zones made of a sequence of protonated carboxyl and hydroxyl groups and hydrophobic interactions between methyl ester groups, which probably did not contribute to aerogel porosity.
- At pH 2 and 3 galacturonic acid is highly deprotonated leading to chains' extension and repulsion. We suppose that when solvent exchange was performed directly on these non-gelled solutions, chains were not forming continuous junction zones which results in high specific surface area.
- Cross-linking with calcium at pH 2 and 3 led to ionic cross-linking of extended and "separated" chains, which resulted in the increase of S_{BET} as compared to physical gels, but not to such high values as for directly coagulated pectin solutions.

The representative examples of the morphology of aerogels from 3 wt% P35 and pore volume are demonstrated in Figures 6 and S8 (Supplementary Material), respectively. The increase of pH led to a denser morphology and strong decrease of pores' size: from around 50-150 nm at pH 1.5 to around 10-50 nm at pH 3 for non-cross-linked pectins (Figure 6). The difference between aerogels made from gels or solutions is significant: contrary to aerogels made from a solution, all aerogels made from gels had macropores. Aerogel from non-cross-linked solution at pH 3 looks very dense but it has porosity around 90 % and is mesoporous, as reflected by high specific surface area (Figure 5b). Strong shrinkage (Figure S7) clearly induced the decrease pores' size. Cross-linking with calcium led to the presence of macropores and thus low density and moderate specific surface area (Figure 5a and 5b).

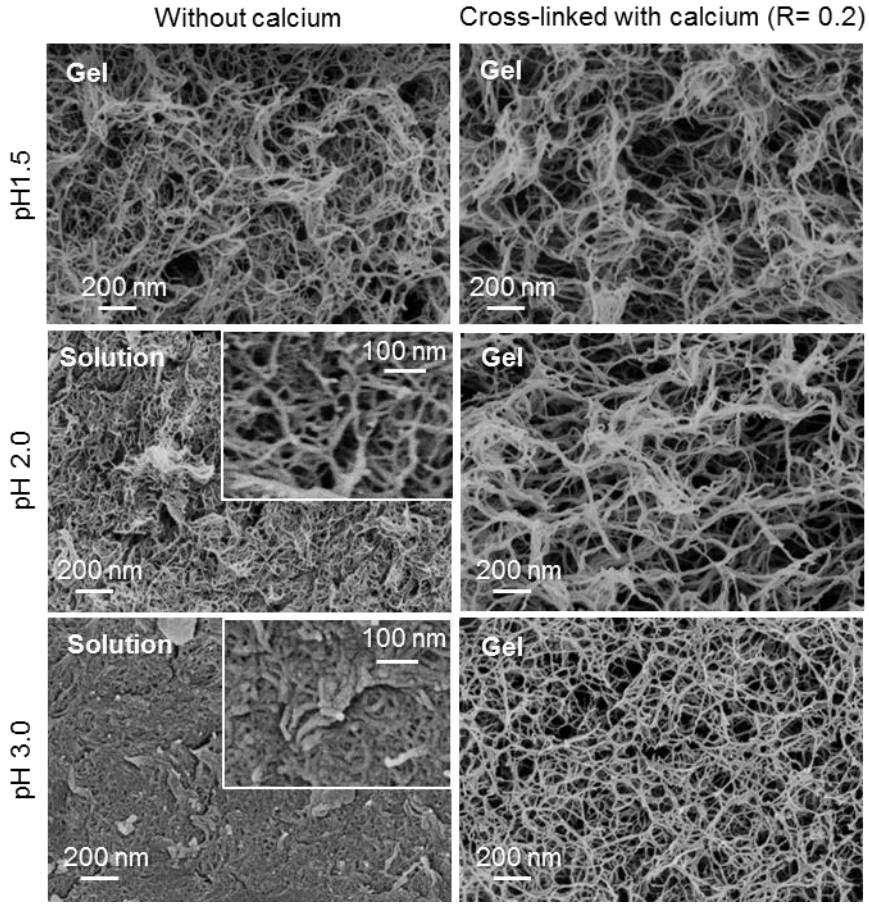

Figure 6

Morphology of aeropectins from P35 dissolved at 3 wt% at various pH, cross-linked with calcium (R = 0.2) and not.

Thermal conductivity of aeropectins as a function of pH is summarized in Figure 7 for 3 wt% pectin, cross-linked with calcium (R = 0.2) and not. In both cases the dependences have a U-shape as in Figure 1 for thermal conductivity vs density. An example of thermal conductivity of non-crosslinked aeropectins as a function of density at various pH is given in Figure S9 of the Supplementary Material. All values are in thermal super-insulating region (conductivity below 0.025 W/m.K). When decreasing pectin concentration to 2 wt% at pH 3, it was possible to obtain the lowest value ever reported for bio-aerogels, 0.0147 ± 0.0002 W/m.K. Aeropectins cross-linked with calcium show conductivity higher than that of non-cross-linked ones, except at pH 1 when they are equal. The reason of this difference is in the microstructure of aeropectins: despite lower density of all cross-linked aerogels as compared to their non-cross-linked counterparts (Figure 5a), the macropores, clearly visible on SEM images (Figure 6), significantly contribute to heat transfer via gaseous phase and are thus unfavorable for the thermal conductivity. Overall, strong gels (at pH 1 and when cross-linked with calcium) that resist shrinkage may be highly porous but are too macroporous for having thermal conductivity below 0.02 W/m.K. Thermal conductivity can be thus used as a measure of structure “finess”. U-shape curve for both types of aeropectins reflects a competition between solid and gaseous phases conductions which depend on aerogel density and morphology, which in turn are controlled by pectin concentration, state of matter before solvent exchange and sample shrinkage.

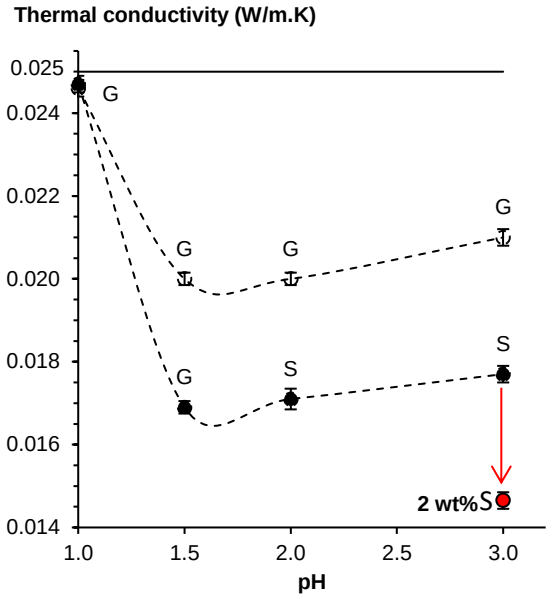

Figure 7

Thermal conductivity in ambient conditions of aeropectins from P35 as a function of pH at pectin concentration 3 wt% and for R = 0 (filled points) and R = 0.2 (open points). One point at pH 3 is for 2 wt% solution. The state of matter before solvent exchange is indicated for each case (solution "S" or gel "G"). Dashed lines are given to guide the eye. Solid line corresponds to the conductivity of air.

3.3.2. Influence of calcium concentration at pH 3

Next we varied calcium concentration keeping pectin at 3 wt% and pH 3 and changing R ratio from 0.05 to 0.2 (eq. 3). With the increase of calcium concentration pectin network was reinforced due to higher cross-linking (Fraeye et al., 2009; Löfgren et al., 2002) and thus it became more resistant leading to lower shrinkage (see Figure S10 in the Supplementary Material) and thus lower density (Figure 8). Specific surface area also decreased with R (see Figure 8), most probably due to increasing amount of ionic non-porous junction zones. It is interesting to see that at R = 0.05 the amount of calcium added was not sufficient to induce

strong ionic gelation, however, calcium influence on density and specific surface area was noticeable.

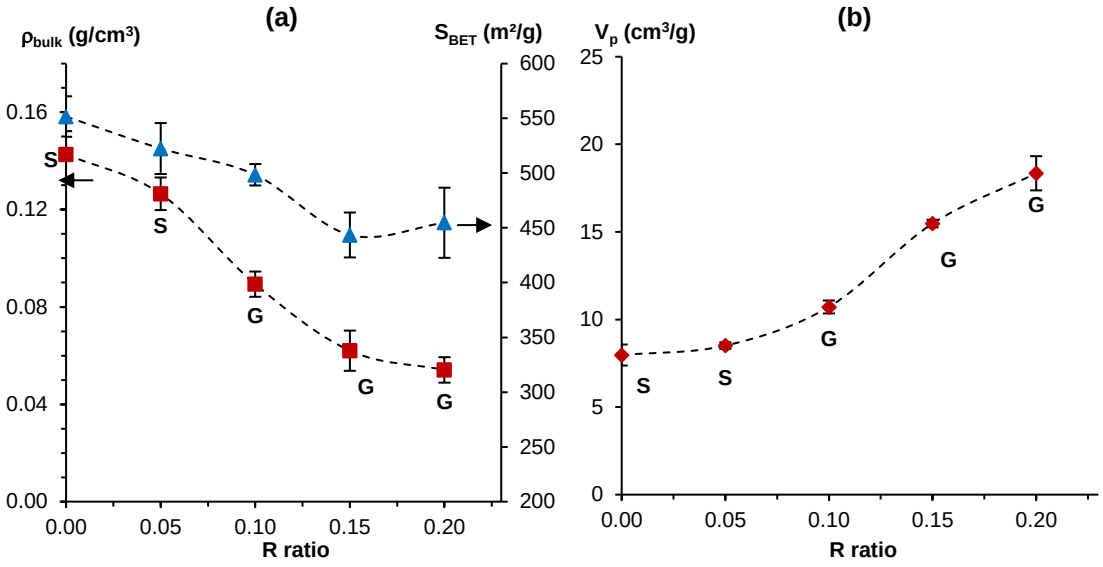

Figure 8

(a) Density (squares) and specific surface area (triangles), (b) pore volume of aeropectins based on P35 dissolved at 3 wt% and pH 3 as a function calcium R ratio. The state of matter before solvent exchange is indicated for each case (solution "S" or gel "G"). Dashed lines are given to guide the eye.

The addition of calcium had a strong impact on pectin morphology as observed by SEM (Figure 9). The higher was R value, the larger were pore sizes due to lower shrinkage. Aeropectin morphology and properties can thus be finely tuned by varying calcium concentration: from very low density with macropores to higher density and compact morphology.

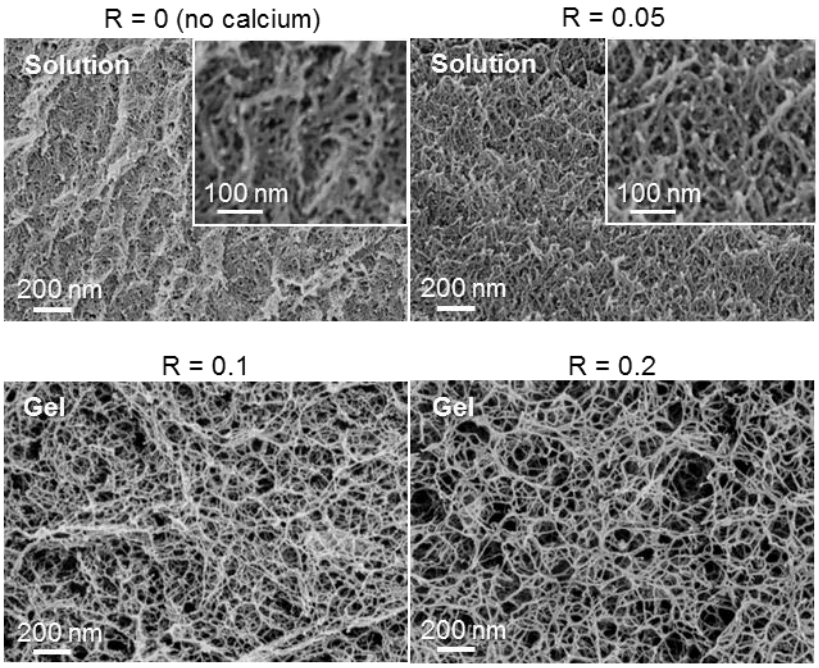

Figure 9

Morphology of aeropectins from P35 dissolved at 3 wt% and pH 3, cross-linked with calcium at different R ratio from R = 0 (no calcium added) to R = 0.2.

Finally, the influence of calcium concentration on thermal conductivity of aeropectins is presented in Figure 10. The same data but as a function of density at various R ratio is shown in Figure S11 of the Supplementary Material. As for the dependences of conductivity vs density (Figure 1) and pH (Figure 7), here it also shows a U-shape. The minimal value obtained was 0.0157 ± 0.0001 W/m.K. The U-shape for calcium cross-linked pectin aerogels shows again that a balance between density and morphology is needed to obtain the lowest thermal conductivity.

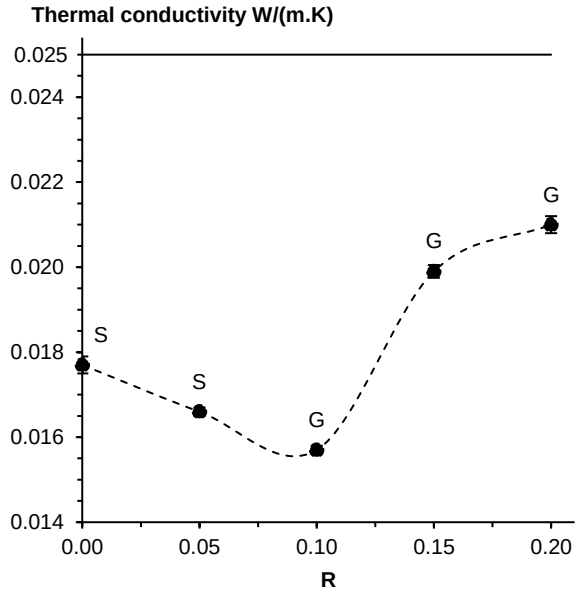

Figure 10

Thermal conductivity in ambient conditions of aeropectins from P35 as a function of R at pectin concentration 3 wt% and pH 3. The state of matter before solvent exchange is indicated for each case (solution "S" or gel "G"). Dashed line is given to guide the eye. Solid line corresponds to the conductivity of air.

4. Conclusions

Pectin aerogels with thermal superinsulating properties were synthesized. To modify aerogel density and morphology and thus understand their influence on aerogel thermal conductivity, pH, concentration of calcium and pectin concentration were varied in a systematic way. Aerogel density was from 0.05 to 0.2 g/cm^3 and specific surface was from 220 to 600 m^2/g.

For the first time a U-shape curve of thermal conductivity vs density was obtained for bio-aerogels synthesized via dissolution-solvent exchange-sc drying route. It shows that the type

of pectin chains' interactions and physical state of matter (solution or gel) are crucial to understand and predict aerogel morphology and properties. More numerous and stronger pectin chains' interactions (ionic vs hydrogen) led to stronger gels (at pH 1 and cross-linked with calcium at all pH studied) which shrinked less during solvent exchange and drying. As a result, aerogels with lower density and high proportion of macropores were obtained. The contribution of the gaseous phase to thermal conductivity was thus high leading to higher thermal conductivity. On the contrary, chains' repulsion at higher pH prevented gelation leading to higher shrinkage and density but also to the reduction of pore size to the level of mesopores. In this case the conduction of the gaseous phase is low thanks to Knudsen effect, but the contribution of the solid backbone increases. A delicate compromise in aeropectin morphology and density is thus needed to get the lowest thermal conductivity. This minimal value of 0.0147 ± 0.0002 W/m.K was found for non-gelled solution at pH 2 and pectin concentration of 2 wt%. Thermal conductivity is a very sensitive parameter reflecting aerogel morphology and can be used to characterize the finesse bio-aerogel structure.

Acknowledgements

Authors are grateful to Cargill, France, for providing raw pectins. We thank Pierre Ilbizian (PERSEE, Mines ParisTech, Sophia-Antipolis, France) for CO_2 supercritical drying, and Suzanne Jacomet (CEMEF, Mines Paristech, Sophia-Antipolis, France) for the guidance in SEM. We wish to acknowledge Sylvie Calas-Etienne and Laurent Bonnet (Laboratoire Charles Coulomb, Université Montpellier 2, Montpellier, France) for pectin skeletal density characterization.

Funding

This research did not receive any specific grant from funding agencies in the public, commercial, or not-for-profit sectors.

References

Biganska, O., & Navard, P. (2005). Kinetics of precipitation of cellulose from cellulose-NMMO-water solutions. *Biomacromolecules*, *6*(4), pages 1948-1953.

Buchtová, N., & Budtova, T. (2016). Cellulose aero-, cryo- and xerogels: towards understanding of morphology control. *Cellulose, 23,* 2585–2595.

Burchard, W., & Ross-Murphy, S. B. (1990). *Physical Networks: Polymers and gels*. Springer Science & Business Media.

Capel, F., Nicolai, T., Durand, D., Boulenguer, P., & Langendorff, V. (2006). Calcium and acid induced gelation of (amidated) low methoxyl pectin. *Food Hydrocolloids*, *20*(6), 901‑907.

Chtchigrovsky, M., Primo, A., Gonzalez, P., Molvinger, K., Robitzer, M., Quignard, F., & Taran, F. (2009). Functionalized chitosan as a green, recyclable, biopolymer-supported catalyst for the [3+2] Huisgen cycloaddition. *Angewandte Chemie (International Ed. in English)*, *48*(32), 5916‑5920.

Diascorn, N., Calas, S., Sallee, H., Achard, P., & Rigacci, A. (2015). Polyurethane aerogels synthesis for thermal insulation – textural, thermal and mechanical properties. *Journal of Supercritical Fluids*, *106*, 76–84.

Djabourov, M., Nishinari, K., & Ross-Murphy, S. B. (2013). *Physical gels from biological and synthetic polymers*. Cambridge: Cambridge Univ. Press.

Druel, L., Bardl, R., Vorwerg, W., & Budtova, T. (2017). Starch Aerogels: A Member of the Family of Thermal Superinsulating Materials. *Biomacromolecules*, *18*(12), 4232‑4239.

Fraeye, I., Doungla, E., Duvetter, T., Moldenaers, P., Van Loey, A., & Hendrickx, M. (2009). Influence of intrinsic and extrinsic factors on rheology of pectin–calcium gels. *Food Hydrocolloids*, *23*(8), 2069‑2077.

Fraeye, I., Duvetter, T., Doungla, E., Van Loey, A., & Hendrickx, M. (2010). Fine-tuning the properties of pectin–calcium gels by control of pectin fine structure, gel composition and environmental conditions. *Trends in Food Science & Technology*, *21*(5), 219‑228.

García-González, C. A., Alnaief, M., & Smirnova, I. (2011). Polysaccharide-based aerogels—Promising biodegradable carriers for drug delivery systems. *Carbohydrate Polymers*, *86*(4), 1425‑1438.

García-González, C. A., Jin, M., Gerth, J., Alvarez-Lorenzo, C., & Smirnova, I. (2015). Polysaccharide-based aerogel microspheres for oral drug delivery. *Carbohydrate Polymers*, *117*, 797‑806.

Gavillon, R., & Budtova, T. (2007). Kinetics of cellulose regeneration from cellulose--NaOH--water gels and comparison with cellulose--N-methylmorpholine-N-oxide--water solutions. *Biomacromolecules*, *8*(2), 424‑432.

Gidley, M. J., Morris, E. R., Murray, E. J., Powell, D. A., & Rees, D. A. (1980). Evidence for two mechanisms of interchain association in calcium pectate gels. *International Journal of Biological Macromolecules*, *2*(5), 332‑334.

Gilsenan, P. M., Richardson, R. K., & Morris, E. R. (2000). Thermally reversible acid-induced gelation of low-methoxy pectin. *Carbohydrate Polymers*, *41*(4), 339‑349.

Gurikov, P., Raman, S. P., Weinrich, D., Fricke, J., & Smirnova, I. (2015). A novel approach to alginate aerogels: carbon dioxide induced gelation. *RSC Advances*, *5*(11), 7812‑7818.

Gurikov, P., & Smirnova, I. (2018). Non-Conventional Methods for Gelation of Alginate. *Gels*, *4*(1), 14.

Hedlund, A., Köhnke, T., & Theliander, H. (2017). Diffusion in Ionic Liquid–Cellulose Solutions during Coagulation in Water: Mass Transport and Coagulation Rate Measurements. *Macromolecules*, *50*(21), 8707‑8719.

Hoepfner, S., Ratke, L., & Milow, B. (2008). Synthesis and characterisation of nanofibrillar cellulose aerogels. *Cellulose*, *15*(1), 121‑129.

Horvat, G., Fajfar, T., Uzunalić, A. P., Knez, Ž., & Novak, Z. (2017). Thermal properties of polysaccharide aerogels. *Journal of Thermal Analysis and Calorimetry*, *127*(1), 363‑370.

Hüsing, N., & Schubert, U. (1998). Aerogels—Airy Materials: Chemistry, Structure, and Properties. *Angewandte Chemie International Edition*, *37*(1‑2), 22‑45.

Innerlohinger, J., Weber, H. K., & Kraft, G. (2006). Aerocellulose: Aerogels and Aerogel-like Materials made from Cellulose. *Macromolecular Symposia*, *244*(1), 126‑135.

Jiménez-Saelices, C., Seantier, B., Cathala, B., & Grohens, Y. (2017). Spray freeze-dried nanofibrillated cellulose aerogels with thermal superinsulating properties. *Carbohydrate Polymers*, *157*, 105‑113.

Jin, H., Nishiyama, Y., Wada, M., & Kuga, S. (2004). Nanofibrillar cellulose aerogels. *Colloids and Surfaces A: Physicochemical and Engineering Aspects*, *240*(1‑3), 63‑67.

Kistler, S. S. (1931). Coherent Expanded-Aerogels. *The Journal of Physical Chemistry*, *36*(1), 52‑64.

Kobayashi, Y., Saito, T., & Isogai, A. (2014). Aerogels with 3D Ordered Nanofiber Skeletons of Liquid-Crystalline Nanocellulose Derivatives as Tough and Transparent Insulators. *Angewandte Chemie International Edition*, *53*(39), 10394‑10397.

Laity, P. R., Glover, P. M., & Hay, J. N. (2002). Composition and phase changes observed by magnetic resonance imaging during non-solvent induced coagulation of cellulose. *Polymer*, *43*(22), 5827–5837.

Löfgren, C., Walkenström, P., & Hermansson, A.-M. (2002). Microstructure and Rheological Behavior of Pure and Mixed Pectin Gels. *Biomacromolecules*, *3*(6), 1144‑1153.

Lootens, D., Capel, F., Durand, D., Nicolai, T., Boulenguer, P., & Langendorff, V. (2003). Influence of pH, Ca concentration, temperature and amidation on the gelation of low methoxyl pectin. *Food Hydrocolloids*, *17*(3), 237‑244.

Masuelli, M. A. (2014). Mark-Houwink Parameters for Aqueous-Soluble Polymers and Biopolymers at Various Temperatures. *Journal of Polymer and Biopolymer Physics Chemistry, 2*, 37-43.

Morris, E. R., Gidley, M. J., Murray, E. J., Powell, D. A., & Rees, D. A. (1980). Characterization of pectin gelation under conditions of low water activity, by circular dichroism, competitive inhibition and mechanical properties. *International Journal of Biological Macromolecules*, *2*(5), 327‑330.

Oakenfull, D., & Scott, A. (1984). Hydrophobic Interaction in the Gelation of High Methoxyl Pectins. *Journal of Food Science, 49*(4), 1093‑1098.

Pircher, N., Carbajal, L., Schimper, C., Bacher, M., Rennhofer, H., Nedelec, J.-M., Liebner, F. (2016). Impact of selected solvent systems on the pore and solid structure of cellulose aerogels. *Cellulose*, *23*(3), 1949‑1966.

Quignard, F., Valentin, R., & Di Renzo, F. (2008). Aerogel materials from marine polysaccharides. *New Journal of Chemistry*, *32*(8), 1300-1310.

Ralet, M.-C., Bonnin, E., & Thibault, J.-F. (2002). Pectins. In *Polysaccharides II: Polysaccharides of Eukaryotes* (Wiley-VCH, Vol. 6). Weinheim: A. Steinbüchel, S. De Baets, E.J. Vandamme.

Ralet, M.-C., Dronnet, V., Buchholt, H. C., & Thibault, J.-F. (2001). Enzymatically and chemically de-esterified lime pectins: characterisation, polyelectrolyte behaviour and calcium binding properties. *Carbohydrate Research*, *336*(2), 117‑125.

Rudaz, C. (2013). *Cellulose and pectin aerogels : towards their nano-structuration* (PhD thesis). Ecole Nationale Supérieure des Mines de Paris.

Rudaz, C., Courson, R., Bonnet, L., Calas-Etienne, S., Sallée, H., & Budtova, T. (2014). Aeropectin: Fully Biomass-Based Mechanically Strong and Thermal Superinsulating Aerogel. *Biomacromolecules*, *15*(6), 2188‑2195.

Seantier, B., Bendahou, D., Bendahou, A., Grohens, Y., & Kaddami, H. (2016). Multi-scale cellulose based new bio-aerogel composites with thermal super-insulating and tunable mechanical properties. *Carbohydrate Polymers*, *138*, 335‑348.

Selmer, I., Kleemann, C., Kulozik, U., Heinrich, S., & Smirnova, I. (2015). Development of egg white protein aerogels as new matrix material for microencapsulation in food. *The Journal of Supercritical Fluids*, *106*, 42‑49.

Sescousse, R., Gavillon, R., & Budtova, T. (2011). Aerocellulose from cellulose–ionic liquid solutions: Preparation, properties and comparison with cellulose–NaOH and cellulose–NMMO routes. *Carbohydrate Polymers*, *83*(4), 1766‑1774.

Ström, A., Schuster, E., & Goh, S. M. (2014). Rheological characterization of acid pectin samples in the absence and presence of monovalent ions. *Carbohydrate Polymers*, *113*, 336‑343.

Thakur, B. R., Singh, R. K., & Handa, A. K. (1997). Chemistry and uses of pectin--a review. *Critical Reviews in Food Science and Nutrition*, *37*(1), 47‑73.

Tkalec, G., Knez, Ž., & Novak, Z. (2015). Formation of polysaccharide aerogels in ethanol. *RSC Advances*, *5*(94), 77362‑77371.

Veronovski, A., Tkalec, G., Knez, Ž., & Novak, Z. (2014). Characterisation of biodegradable pectin aerogels and their potential use as drug carriers. *Carbohydrate Polymers*, *113*, 272‑278.

Voragen, F., Schols, H., & Visser, R. (Ed.). (2003). *Advances in Pectin and Pectinase Research*. Dordrecht: Springer Netherlands.

Walkinshaw, M. D., & Arnott, S. (1981). Conformations and interactions of pectins: II. Models for junction zones in pectinic acid and calcium pectate gels. *Journal of Molecular Biology*, *153*(4), 1075‑1085.

White, R. J., Budarin, V. L., & Clark, J. H. (2010). Pectin-Derived Porous Materials. *Chemistry – A European Journal*, *16*(4), 1326‑1335.

Wijmans, J. G., Altena, F. W., & Smolders, C. A. (1984). Diffusion during the immersion precipitation process. *Journal of Polymer Science: Polymer Physics Edition*, *22*(3), 519‑524.

Wijmans, J. G., Baaij, J. P. B., & Smolders, C. A. (1983). The mechanism of formation of microporous or skinned membranes produced by immersion precipitation. *Journal of Membrane Science*, *14*(3), 263‑274.

Supplementary material

Thermal conductivity/structure correlations in thermal super-insulating pectin aerogels

Sophie Groult, Tatiana Budtova*

MINES ParisTech, PSL Research University, Center for Materials Forming (CEMEF),

UMR CNRS 7635, CS 10207, 06904 Sophia Antipolis, France

Figure S1

Illustration of solvent exchange for non-gelled solutions:

a) pictures of non-gelled P35 solution (3 wt%, pH 3), solvent exchange, “alcogel” and aerogel;

b) schematic presentation of phase separation occurring during solvent exchange

(a)

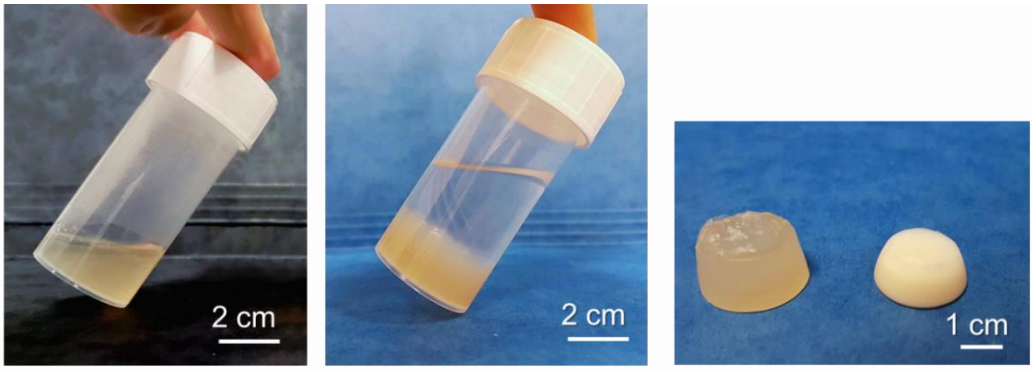

3 wt% P35 solution, pH 3

Solvent exchange: ethanol is on the top of solution diffusing inside

Pectin “alcogel” before drying (left) and aerogel after drying (right)

...

(b)

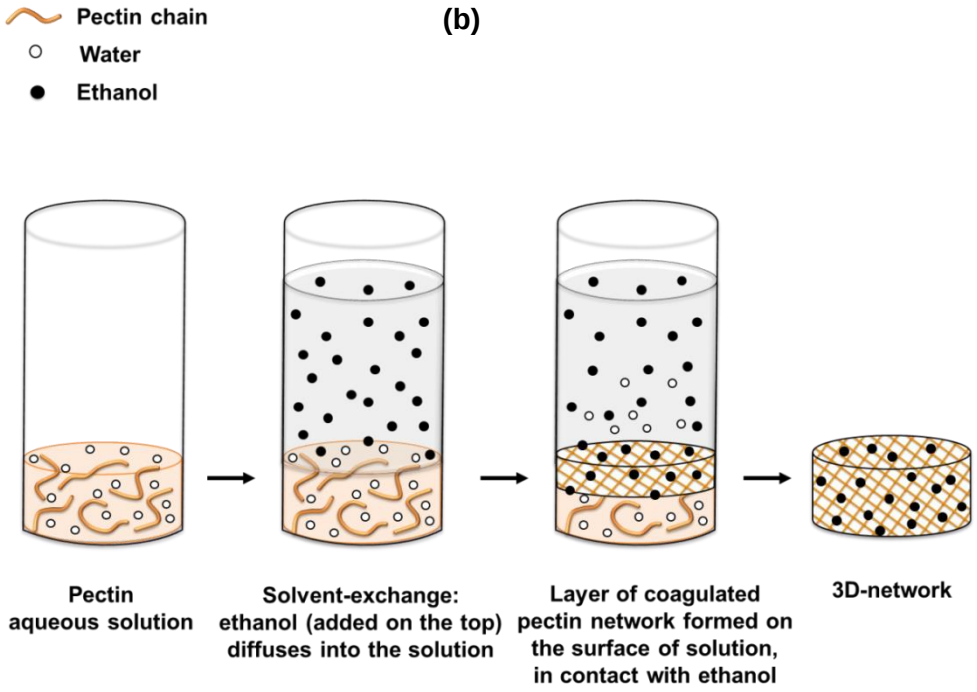

Figure S2

Images of pectin gel and aerogels (the scale is the same on all pictures):

a) From gel to aerogel: P35 dissolved at 3 wt% at pH 1.5 (no calcium added),

b) Aeropectins made from P35 dissolved at 3 wt%, at pH 3, 2 and 1.5, with and without calcium (R = 0.2)

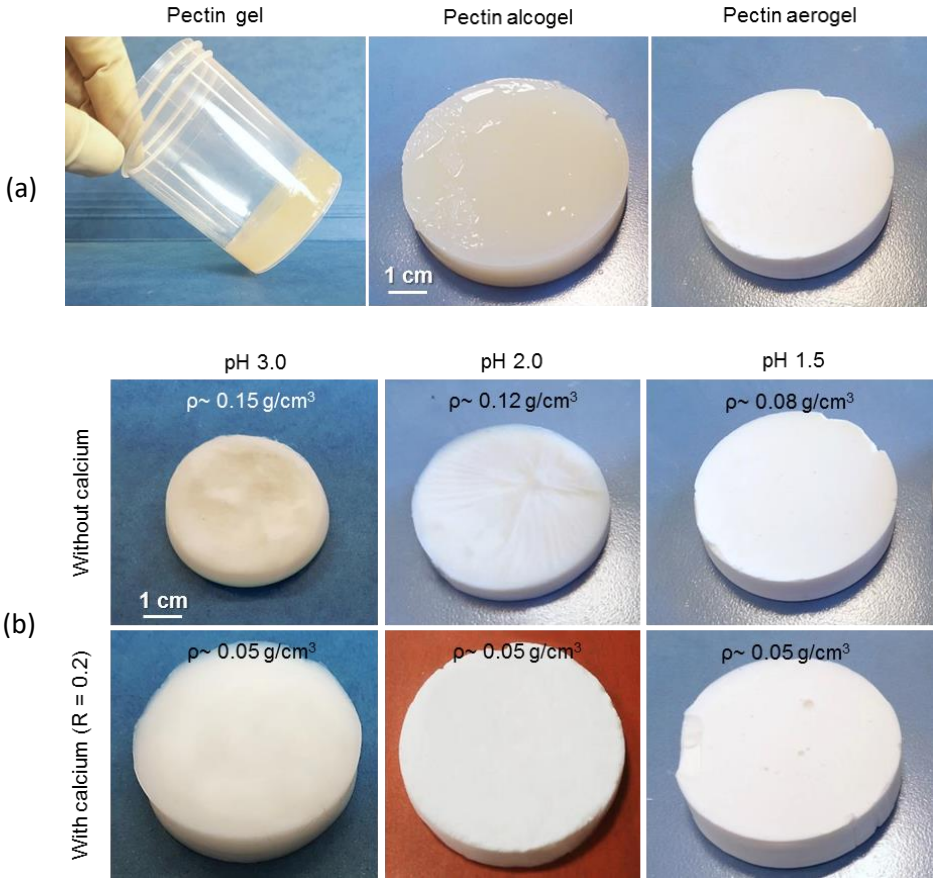

Figure S3.

Example of BJH analysis of pectin aerogel made from 3 wt% of P35 at pH 3.0 with calcium at R = 0.2:

a) adsorption/desorption curves,

b) structural parameters obtained and

c) SEM image of this sample

(a)

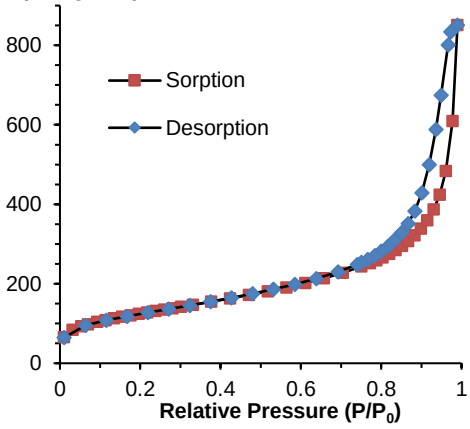

(b)

Cumulative surface area of pores S_{BET} (m^2/g)	444.3 ± 2.2
Cumulative surface area of pores S_{BJH} (m^2/g)	355 (adsorption) 401 (desorption)
Cumulative pore volume of pores $V_{p,BJH}$ (cm^3/g)	1.25

(c)

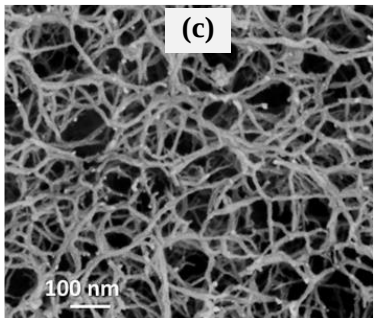

Pore volume V_p calculated with eq. 5 is 18.3 cm^3/g.

Table S1. Characteristics of all aeropectins synthesised in the work. The state of matter solution before solvent-exchange "S" or gel "G" is given in each case.

Pectin DE (%)	Pectin wt%	pH	R ratio	State of matter	Shrinkage after solvent-exchange (%)	Volumetric shrinkage (%)	Bulk density (g/cm^3)	Porosity (%)	Pore volume (cm3 / g)	Specific surface area (m^2/g)	Thermal conductivity (W/mK)
70	3	1.0	0	S	9.0 ± 1.7	46.0 ± 1.8	0.049 ± 0.002	96.7 ± 0.2	18.23 ± 0.52	329 ± 9	0.01920 ± 0.00015
70	3	1.0	0.20	S	12.0 ± 1.3	48.3 ± 2.5	0.055 ± 0.004	96.3 ± 0.3	18.18 ± 0.66	326 ± 9	0.02020 ± 0.00015
59	3	1.0	0	S	10.0 ± 2.3	57.8 ± 1.9	0.069 ± 0.006	95.4 ± 0.6	15.00 ± 0.30	396 ± 13	0.01890 ± 0.00020
59	3	1.0	0.20	S	16.0 ± 1.1	53.9 ± 1.9	0.069 ± 0.003	95.4 ± 0.4	15.37 ± 0.16	371 ± 6	0.01860 ± 0.00020
56	3	1.0	0	S	17.8 ± 1.2	54.5 ± 1.0	0.051 ± 0.001	96.6 ± 0.1	18.93 ± 0.24	326 ± 13	0.01970 ± 0.00015
56	3	1.0	0.20	S	18.7 ± 1.3	40.4 ± 1.8	0.048 ± 0.001	96.8 ± 0.1	20.02 ± 0.26	321 ± 20	0.02030 ± 0.00010
35	3	1.0	0	G	17.0 ± 0.8	50.8 ± 2.7	0.051 ± 0.003	96.6 ± 0.5	17.08 ± 0.53	238 ± 10	0.02470 ± 0.00020
35	3	1.0	0.20	G	20.2 ± 0.5	38.6 ± 1.6	0.053 ± 0.001	96.5 ± 0.2	18.73 ± 0.30	219 ± 9	0.02460 ± 0.00020
35	3	1.5	0	G	30.3 ± 1.2	65.4 ± 1.2	0.075 ± 0.005	95.0 ± 0.5	12.34 ± 0.81	249 ± 24	0.01690 ± 0.00015
35	3	1.5	0.20	G	20.1 ± 0.6	41.4 ± 1.4	0.048 ± 0.002	96.8 ± 0.1	19.60 ± 0.18	257 ± 21	0.02000 ± 0.00015
35	2	2.0	0	S	39.0 ± 2.9	80.6 ± 3.6	0.092 ± 0.015	93.9 ± 2.0	10.20 ± 0.27	*274* ± 33	0.01570 ± 0.00020

35	3	2.0	0	S	28.1	±	3.5	73.8	±	2.5	0.127	±	0.007	91.5	±	1.0	9.29	±	0.30	399	±	6	0.01710	±	0.00025
35	4	2.0	0	G	33.3	±	1.9	69.8	±	1.7	0.119	±	0.005	92.1	±	0.4	7.98	±	0.31	416	±	28	0.01700	±	0.00010
35	6	2.0	0	G	17.4	±	2.1	67.3	±	1.0	0.166	±	0.013	89.0	±	1.2	5.77	±	0.35	444	±	21	0.02000	±	0.00025
35	2	2.0	0.20	G	20.9	±	2.8	40.4	±	2.5	0.031	±	0.004	97.9	±	0.3	30.01	±	1.79	*267*	±		0.02150	±	0.00020
35	3	2.0	0.20	G	7.3	±	1.2	34.5	±	3.0	0.048	±	0.001	96.8	±	0.5	19.22	±	1.08	317	±	12	0.02000	±	0.00015
35	4	2.0	0.20	G	11.0	±	2.0	29.9	±	0.6	0.055	±	0.001	96.4	±	0.9	17.12	±	0.38	342	±	22	0.02040	±	0.00015
35	6	2.0	0.20	G	8.0	±	1.8	32.6	±	2.7	0.082	±	0.006	94.5	±	0.7	12.85	±	0.98	357	±	18	0.02130	±	0.00015
35	2	3.0	0	S	44.2	±	1.4	81.4	±	2.3	0.103	±	0.007	93.1	±	0.3	9.15	±	0.33	541	±	24	0.01465	±	0.00020
35	3	3.0	0	S	23.1	±	4.8	79.7	±	3.9	0.143	±	0.010	90.5	±	0.5	7.97	±	0.60	552	±	18	0.01770	±	0.00020
35	4	3.0	0	S	20.6	±	5.3	68.4	±	2.8	0.127	±	0.010	91.5	±	0.9	7.68	±	0.48	601	±	16	0.01620	±	0.00020
35	6	3.0	0	G	6.8	±	1.4	71.5	±	0.5	0.182	±	0.015	87.9	±	1.7	5.98	±	0.32	529	±	22	0.02170	±	0.00015
35	3	3.0	0.05	S	40.0	±	5.6	75.4	±	3.4	0.127	±	0.007	91.6	±	0.2	8.51	±	0.19	522	±	23	0.01660	±	0.00010
35	3	3.0	0.10	G	33.1	±	1.0	63.9	±	1.8	0.089	±	0.005	94.0	±	0.2	10.71	±	0.37	499	±	10	0.01570	±	0.00010
35	3	3.0	0.15	G	26.9	±	0.9	51.8	±	1.5	0.062	±	0.008	95.9	±	0.1	15.48	±	0.21	444	±	21	0.01990	±	0.00015
35	3	3.0	0.20	G	16.8	±	2.1	39.2	±	2.8	0.054	±	0.005	96.4	±	0.2	18.35	±	0.98	455	±	32	0.0210	±	0.00020

Figure S4.

Volume shrinkage of pectin aerogels after solvent exchange (squares) and overall volume shrinkage after sc drying (triangles) as a function of P35 concentration at pH 2. Filled points correspond to non-cross-linked sample, open points – when calcium was added (R = 0.2). The state of matter before solvent exchange is indicated for each case (solution "S" or gel "G"). Lines are given to guide the eye.

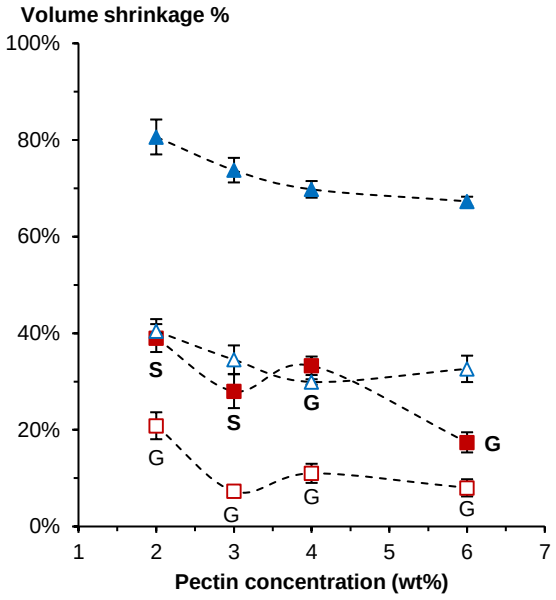

Figure S5

Influence of non-crosslinked pectin concentration and state of the matter before solvent exchange (solution "S" or gel "G") on bulk density (squares) and specific surface area (triangles) of aeropectins based on P35 dissolved at pH 3(without addition of calcium). Solid line is theoretical density corresponding to zero volume shrinkage. Dashed lines are given to guide the eye.

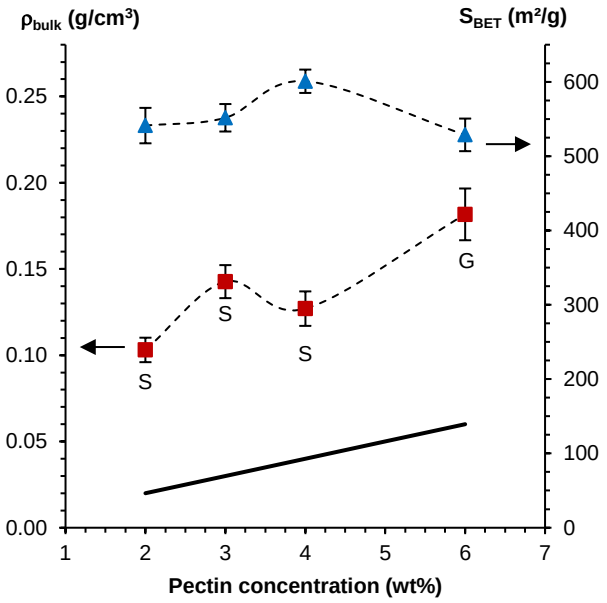

Figure S6

Thermal conductivity in ambient conditions of aeropectins from P35 as a function of density, with pectin concentration varying from 2 wt% to 6 wt%, at pH 3 (squares) and pH 2 (diamonds), both without calcium. The state of matter before solvent exchange is indicated for each case (solution "S" or gel "G"). Dashed line is given to guide the eye. Solid line corresponds to the conductivity of air.

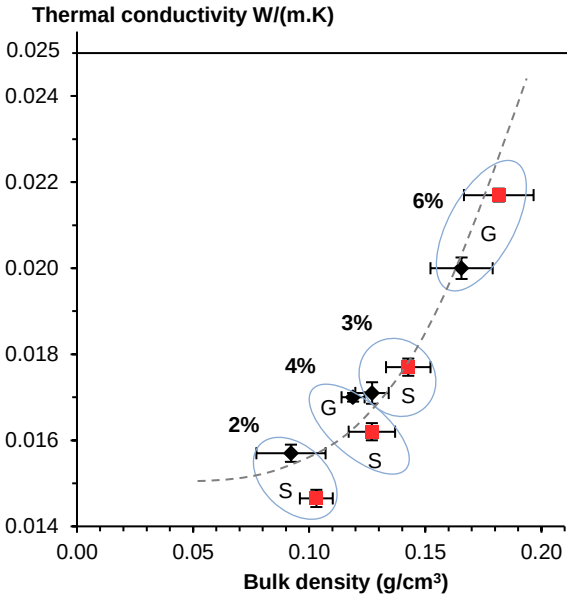

Figure S7

Influence of pH, presence of calcium (R = 0.2) (dotted bars) and state of matter before solvent exchange (solution "S" or gel "G") on P35 shrinkage after solvent exchange (white bars) and after sc drying (grey bars). Initial polymer concentration was 3 wt%.

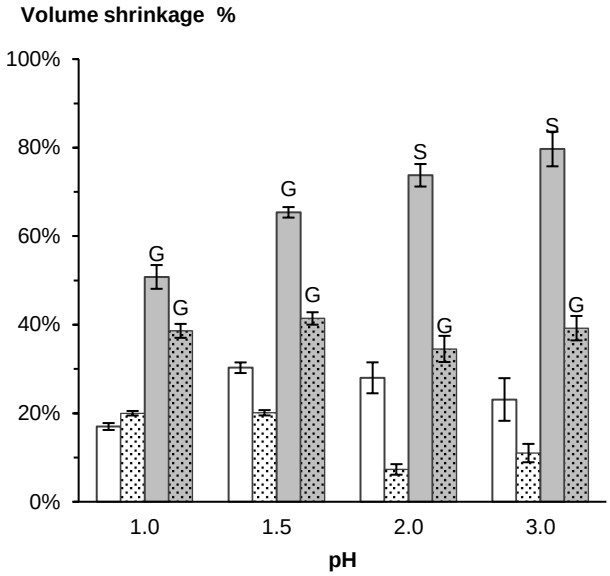

Figure S8

Pore volume of aeropectins made from 3 wt% of P35 dissolved at different pH. Filled points correspond to non-cross-linked samples, open points – when calcium was added (R = 0.2). The state of matter before solvent exchange is indicated for each case (solution "S" or gel "G"). Dashed lines are given to guide the eye.

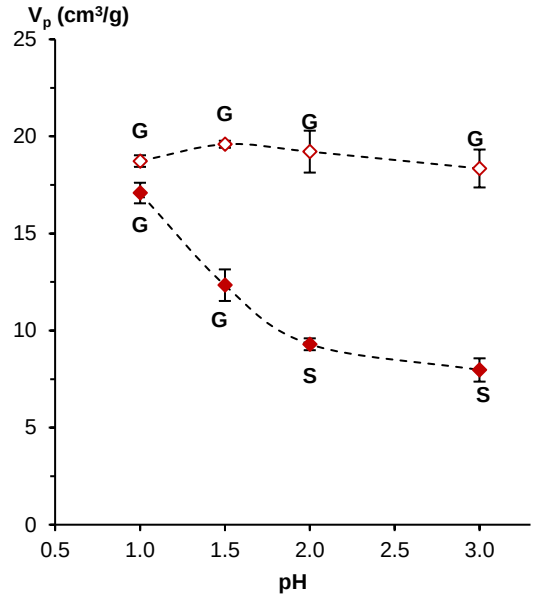

Figure S9

Thermal conductivity in ambient conditions of aeropectins made from 3 wt% of P35 as a function of density with pH varying from 1 to 3 and without calcium. The state of matter before solvent exchange is indicated for each case (solution "S" or gel "G"). Dashed line is given to guide the eye. Solid line corresponds to the conductivity of air.

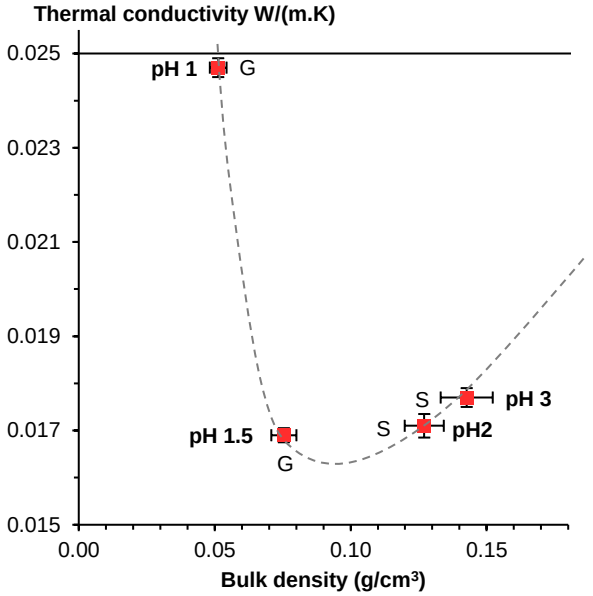

Figure S10

Influence of calcium concentration (R ratio) and state of matter before solvent exchange (solution “S” or gel “G”) on P35 shrinkage after solvent exchange (white bars) and after sc drying (grey bars). Polymer concentration in solution was 3 wt% and pH was 3.

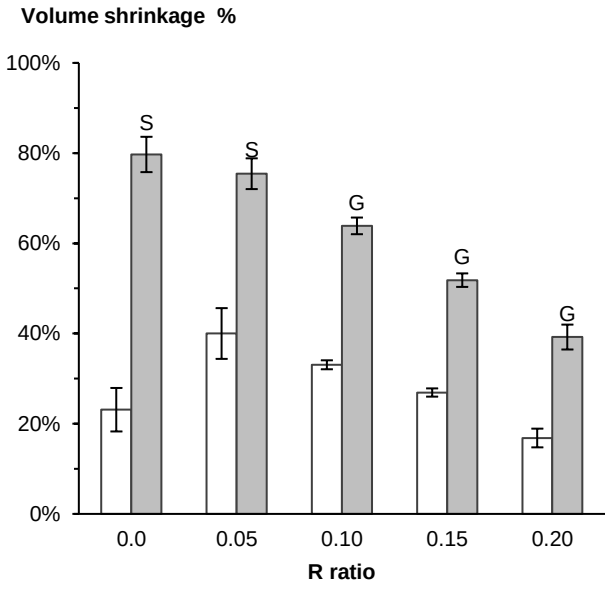

Figure S11

Thermal conductivity in ambient conditions of aeropectins from P35 as a function of density at various R, at pectin concentration 3 wt% and pH 3. The state of matter before solvent exchange is indicated for each case (solution “S” or gel “G”). Dashed line is given to guide the eye. Solid line corresponds to the conductivity of air.